Semicond. Sci. Technol. 10 (1995) 1680–1688. Printed in the UK

Current–voltage characteristics and barrier parameters of Pd_2Si/p-Si(111) Schottky diodes in a wide temperature range

Subhash Chand and Jitendra Kumar†

Materials Science Programme, Indian Institute of Technology, Kanpur-208016, UP, India

Received 3 April 1995, in final form 12 July 1995, accepted for publication 28 July 1995

Abstract. Current–voltage characteristics of Pd_2Si/p-Si(111) Schottky barrier diodes studied over a wide temperature range (60–201 K) are shown to follow a thermionic emission–diffusion mechanism under both the forward and the reverse bias conditions. The barrier parameters as evaluated from the forward I–V data reveal a decrease of zero-bias barrier height (ϕ_{b0}) but an increase of ideality factor (η) and series resistance (R_s) with decrease in temperature. Moreover, the changes in ϕ_{b0}, η and R_s become quite significant below $\sim$100 K. An $\ln(I_s/T^2)$ versus $1/T$ plot is found to fit well with two straight lines in different temperatures regimes giving an activation energy of 0.33 eV (201–107 K) and 0.24 eV (below 107 K) and an effective Richardson constant of 33 A cm^{-2} K^{-2}. However, the activation energy of 0.33 eV corresponds to the zero-bias barrier height at absolute zero. An $\ln(I_s'/T^2)$ versus $1/\eta T$ plot is suggested to obtain the flat-band barrier height and the effective Richardson constant; the corresponding values obtained are 0.401 eV and 32.2 A cm^{-2} K^{-2} respectively. It is shown that the 'T_0 effect' cannot account for the apparent increase in ideality factor and decrease of barrier height at low temperatures. Finally, the decrease of barrier height with voltage under the reverse bias condition is attributed mainly to interfacial layer effects with a small contribution due to image force lowering.

1. Introduction

The important aspect of metal–semiconductor junctions is the process which determines the flow of charge carriers over the barrier from the semiconductor to the metal and vice versa. Detailed knowledge of the conduction process involved is essential to extract barrier parameters, namely barrier height, ideality factor and series resistance. Analysis of the current–voltage (I–V) characteristics of the Schottky barrier measured only at room temperature does not give detailed information about the conduction process and the nature of barrier formed at the metal–semiconductor interface. In fact, it neglects many possible effects that cause non-ideality in the diode I–V characteristics and, in general, reduce the barrier height. The temperature dependence of the I–V characteristics gives a better picture of various conduction mechanisms and allows one to understand different aspects that shed light on the validity of various processes involved. Moreover, Schottky diodes with low barrier heights have found applications in devices operating at cryogenic temperatures as infrared detectors and sensors in thermal imaging [1–3]. So, information about their electrical characteristics at low temperatures is vital for better understanding which will enable us to tailor the devices to particular requirements.

The I–V characteristics of Schottky barrier diodes formed by depositing various metals such as Ir, Pt, Cr, Er, W, Cu, Ti and Au on silicon have been studied extensively over a wide temperature range [4–15]. However, a few brief reports exist in the literature on palladium silicide-based Schottky barrier diodes [16–18]. For example, Chin et al [16] studied Pd_2Si Schottky barrier diodes on n-type silicon at 300 K and on p-type silicon at 84 K only. Werner and Guttler [17] reported some data on Pd_2Si Schottky barrier diodes as well while describing the temperature dependence of barrier height for various metals on n-type silicon. Chand and Kumar [18] in a recent note gave a brief account of their values of barrier height and ideality factor obtained from the forward bias I–V characteristics of Pd_2Si Schottky diodes on p-type silicon in the temperature range 60–201 K. Obviously, details are not available on the current transport process and other properties of the Pd_2Si/p-Si

† To whom all correspondence should be addressed.

0268-1242/95/121680+09 $19.50

Schottky barrier diodes over a wide temperature range despite their importance in silicon device technology and potential applications as infrared detectors and sensors in thermal imaging [1–3]. An attempt has therefore been made here to deal at length with various aspects such as *I–V* characteristics, barrier height, ideality factor, current transport mechanism, barrier lowering, temperature dependence, etc of the Pd_2Si/p-Si(111) Schottky barrier diodes under both forward and reverse bias conditions in the temperature range 60–201 K.

2. Experiment

The Pd_2Si Schottky barrier diodes were prepared on p-type boron-doped silicon wafers of (111) orientation. The p/p^+ silicon wafer used had a 12–18 μm thick epitaxial p-layer of resistivity 2–3 Ω cm over the underlying heavily doped p^+ region of resistivity 0·01 Ω cm. The wafers were first degreased with soap solution and then cleaned with organic solvants, namely trichloroethylene, acetone and methanol in succession, in an ultrasonic cleaner, rinsed in deionized water and dried. Ohmic contacts were established on the back (i.e. the p^+) side of the silicon wafer by depositing aluminium and subsequent annealing in nitrogen at 450 °C for 30 min. The palladium film (thickness ~800 Å) was subsequently deposited by employing an electron beam evaporation source onto the epitaxial p-layer (i.e. front side) of the precleaned silicon wafer through holes (1 mm ∅) in the metal mask and annealed at 450 °C in a vacuum of $\sim 10^{-5}$ mbar for 2 h to form a Schottky junction. Before metal deposition wafers were etched in dilute hydrofluoric acid ($HF : H_2O = 1 : 10$) for removal of the silicon dioxide layer usually formed on silicon. For measuring the *I–V* characteristics of the Schottky diodes use was made of a programmable voltage source (Keithley model 230), an autoranging picometer (Keithley model 485) and a personal computer (Zenith PC-XT). To ensure steady-state conditions a delay of few seconds was observed between subsequent measuring steps. Moreover, an average of three current readings was taken at each voltage step. For the study of temperature dependence of the *I–V* characteristics a closed-cycle helium refrigerator (CTI-cryotronics model 22C) equipped with a temperature controller (Lake Shore model 805) was employed. The actual temperature of the device was also monitored by placing a copper–constantan thermocouple close to the device and measuring the e.m.f. with a microvoltmeter (Keithley model 197). A Rich Seifert ISO-Debyeflex 2002 x-ray diffractometer with Cu Kα radiation ($\lambda = 1.5418$ Å) was used to identify the silicide phase formed during the heat treatment.

3. Basic equations

The current through a Schottky barrier diode at a forward bias 'V', based on the thermionic emission–diffusion theory, is given by the relation [19, 20]

$$I = A_d A^{**} T^2 \exp\left(\frac{-q\phi_b}{kT}\right)\left[\exp\left(\frac{qV}{kT}\right) - 1\right] \quad (1)$$

where A_d is the diode area, A^{**} is the effective Richardson constant. T is the temperature in Kelvin, k is the Boltzmann constant, q is the electronic charge and ϕ_b is the barrier height. However, the barrier height invariably increases with the *forward bias*. If the barrier height is assumed to vary linearly with bias, one writes

$$\phi_b(V) = \phi_{b0} + \gamma V \quad (2)$$

where ϕ_{b0} is the barrier height at zero bias and γ ($= \partial\phi_b/\partial V$) is positive. Using substitution (2), equation (1) becomes

$$I = I_s \exp\left(\frac{-\gamma q V}{kT}\right)\left[\exp\left(\frac{qV}{kT}\right) - 1\right] \quad (3)$$

where

$$I_s = A_d A^{**} T^2 \exp\left(\frac{-q\phi_{b0}}{kT}\right) \quad (4)$$

is termed the saturation current at zero bias. Now, introducing a parameter η such that $1/\eta = 1 - \gamma$, equation (3) can be written as

$$I = I_s \exp\left(\frac{qV}{\eta kT}\right)\left[1 - \exp\left(\frac{-qV}{kT}\right)\right]. \quad (5)$$

When $\eta = 1$ (or $\gamma = 0$), equation (5) reduces to the case of pure thermionic emission–diffusion (i.e. equation (1)). The parameter η is called the ideality factor and usually has a value greater than unity. This amounts to extra current arising due to other mechanisms and/or variation in barrier height. For example, thermionic-field emission, generation–recombination, tunnelling, interface impurities, interfacial oxide layer, image forces all tend to increase current, and hence η, above unity. Also, a correlation exists between η and ϕ_b which is discussed later. The neutral region of the semiconductor (between the depletion region and back ohmic contact) offers resistance (R_s) and so a significant voltage drop occurs across that at large forward currents. This amounts to a reduction of the voltage across the barrier region from that actually applied to the terminals of the diode. This is accounted for by replacing the V by $V - IR_s$ in equation (5). The current equation them becomes

$$I = I_s \exp\left(\frac{q(V - IR_s)}{\eta kT}\right)\left[1 - \exp\left(\frac{-q(V - IR_s)}{kT}\right)\right] \quad (6)$$

In such a situation a plot of $\ln(I)$ versus V deviates from a straight line at high forward voltages.

4. Results and discussion

X-ray diffraction analysis revealed the formation of Pd_2Si during the heat treatment. The Pd_2Si phase belongs to the hexagonal system and exhibits a preferred orientation with its basal plane lying parallel to the (111) plane of the underlying silicon wafer.

4.1. Forward I–V characteristics

The forward current–voltage (I–V) characteristics of Pd_2Si Schottky barrier diodes on p-type Si(111) in the temperature range 60–201 K are shown in figure 1. These are indeed linear over several orders of current at lower temperatures. Figure 1 clearly depicts that the ln I versus V plot becomes progressively straighter over a wide bias range as the temperature is lowered. Such an observation suggests the dominance of the thermionic emission–diffusion mechanism for current transport. This feature is quite consistent with the fact that the thermionic emission condition ($\mu E \gg v/4$; μ being the mobility of the charge carriers, E the electric field in the depletion region and v the average velocity of the carriers) is valid only at low temperatures and high electric fields E (i.e. correspondingly large forward bias) for Schottky barriers

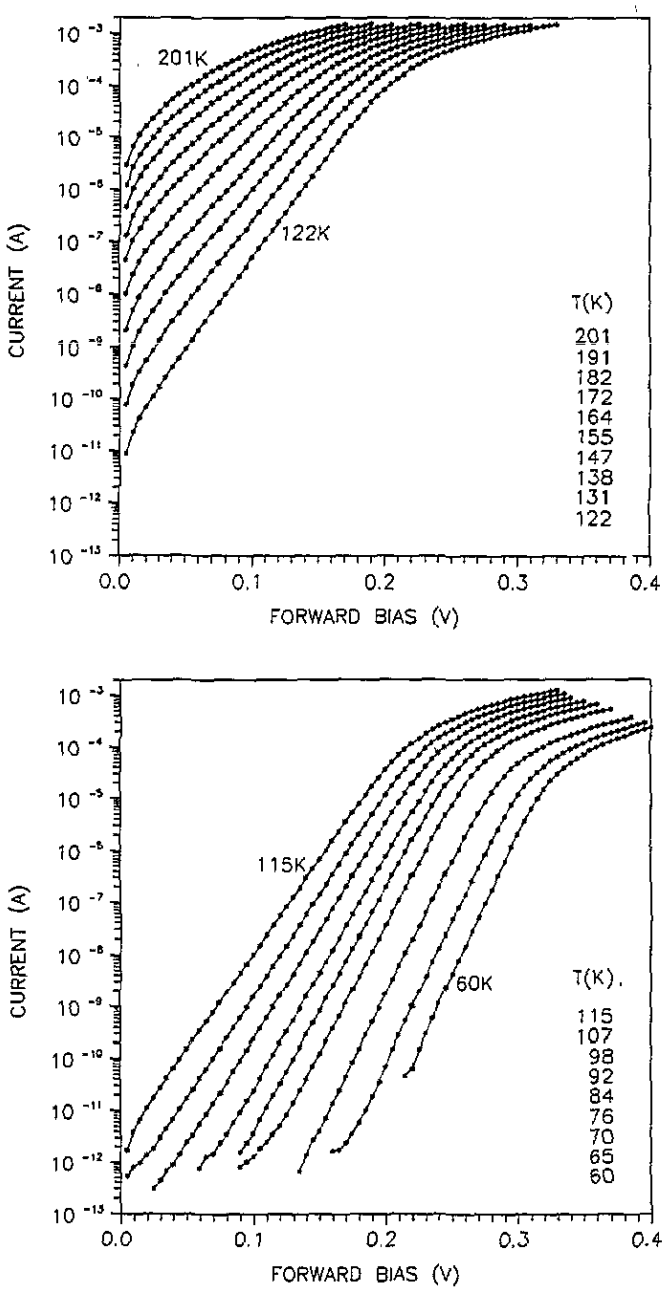

Figure 1. Current–voltage characteristics of the Pd_2Si/p-Si Schottky barrier diodes at different temperatures.

on p-type silicon [20]. At temperatures above 201 K, the junction tends to become nearly ohmic. This is perhaps due to Schottky junctions exhibiting low barrier heights on p-type silicon. Also, the increase in the slope of the straight line portion of the I–V curve and the shifting of the plot towards the higher voltage side with decrease in temperature (figure 1) are in agreement with equations (5) or (6).

A program in BASIC has been developed to fit the experimental I–V data in the thermionic emission–diffusion current equation (6). It involves iteration and takes I_s, η and R_s as adjustable parameters. The steps involved can be summarized as follows. An $\ln\{I/[1-\exp(-qV/kT)]\}$ versus V plot is made (equation (5)) at each temperature mainly to cover the wide bias range including the regime $V < 3kT/q$ where the $1-\exp(-qV/kT)$ factor is effective. The straight line portion of such a plot corresponds to the thermionic-emission diffusion current with the intercept at the ordinate giving ln I_s and the slope the ideality factor (η). However, the nature of the plot usually makes the straight line portion quite subjective and leads to uncertainties/errors in values of ln I_s determined by extrapolation. So, the computer program is initially run by assuming the ideality factor (η) to be unity and the series resistance (R_s) to be zero, principally to obtain an approximate value of I_S that fits the experimental data well. This I_s is then introduced into equation (6) and the program is run again to determine the value of R_s. Iteration continues until one finds a set of I_s, η and R_s values that fit the experimental data at each temperature over as wide a range of forward biases as possible with minimum deviation.

4.1.1. Zero-bias barrier height, ideality factor and series resistance. The zero-bias barrier height (ϕ_{b0}) can now be evaluated from I_s data by substituting the values of the effective Richardson constant A^{**}, diode area A_d and temperature T. The sensitivity of the method is dependent on the precise knowledge of the constant A^{**}, the diode area A_d and the temperature T. In this case, A_d has been determined by examining the diode area under reflection in a Leitz ASM 68 K image analyser, A^{**} is taken as 32 A cm^{-2} K^{-2} for p-type silicon [20] and the temperature T is monitored with a sensitivity of ± 1 K. Thus, ϕ_{b0} is found at each temperature from equation (4).

The zero-bias barrier height ϕ_{b0} as a function of temperature is shown in figure 2. It clearly shows that ϕ_{b0} initially decreases slowly with the fall in temperature but declines sharply below ~ 107 K. The ideality factor (η) versus temperature plot (figure 3) indicates a nearly constant value of 1.2 up to 107 K but significantly higher values at low temperatures (e.g. $\eta = 1.52$ at 60 K). Both the increase in η and decrease in barrier height with decrease in temperature are *at first sight* indicative of deviation from the pure thermionic emission–diffusion theory and arise perhaps due to current resulting by other processes, namely tunnelling through the barrier and recombination in the depletion region. The parameter that determines the relative importance of tunnelling

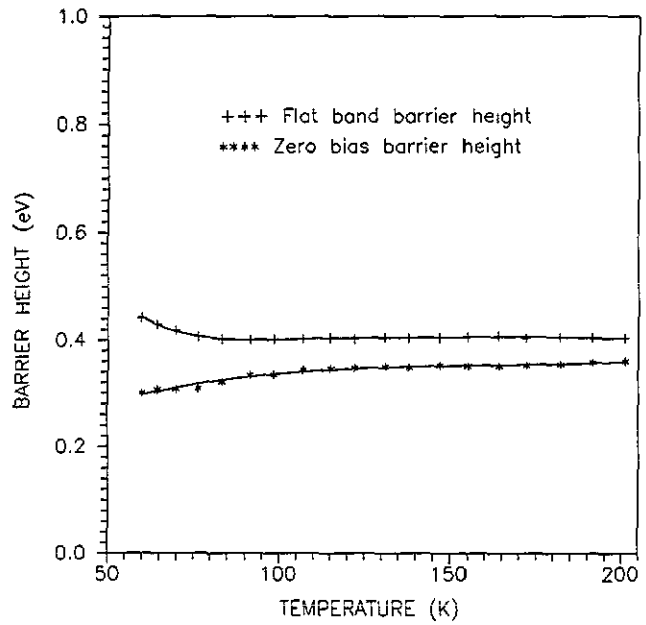

Figure 2. Variation of the zero-bias barrier height (ϕ_{b0}) and flat-band barrier height (ϕ_b^f) with temperature. Notice a significant decrease in ϕ_{b0} below 107 K and a substantial increase in ϕ_b^f below 76 K. Also, ϕ_b^f essentially remains constant over a wide temperature range (76–201 K).

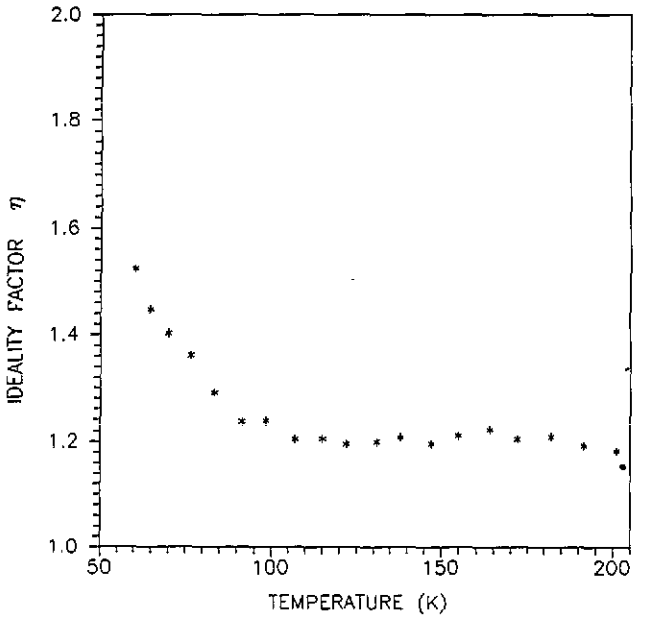

Figure 3. Temperature dependence of the ideality factor η. There is sharp increase in η as the temperature falls below 107 K.

(thermionic-field emission or field emission) and thermionic emission–diffusion is given by [20]

$$E_{00} = \frac{h}{4\pi}\left(\frac{N_A}{m_h^* \varepsilon_s}\right)^{1/2} = 18.5 \times 10^{-15}\left(\frac{N_A}{m_r \varepsilon_r}\right)^{1/2} \text{eV} \quad (7)$$

where m_h^* ($=m_r m_0$) is the effective mass of holes, ε_s ($=\varepsilon_r \varepsilon_0$) is the permittivity of the semiconductor, m_0 is the electron rest mass and N_A is the acceptor concentration in m^{-3}. Field emission (FE) becomes important when $E_{00} \gg kT$, whereas thermionic-field emission (TFE) dominates when $E_{00} \sim kT$, and thermionic emission–diffusion (TED) if $E_{00} \ll kT$. N_A is 5.16×10^{21} m^{-3} for the p-Si wafer used. The corresponding E_{00} value is 0.5 meV with $m_r = 0.56$ and $\varepsilon_r = 11.9$. This leads to E_{00}/kT equal to 0.06 at 100 K. Obviously, the current expected in this situation is mainly due to thermionic emission–diffusion. Also, TFE causes a reduction in the barrier height by an amount [20]

$$\Delta\phi = (3/2)^{2/3} E_{00}^{2/3} V_d^{1/3} \quad (8)$$

where V_d stands for the voltage corresponding to the band bending. Thus, for $E_{00} = 0.5$ meV and assuming $V_d = 0.3$ V, barrier lowering of 5.5 meV should occur, which is very small. The current–voltage relationship in the case of tunnelling through the barrier is of the form [20]

$$I_t = I_{t0} \exp\left(\frac{qV}{E_0}\right)\left[1 - \exp\left(\frac{-qV}{kT}\right)\right] \quad (9)$$

where

$$E_0 = E_{00} \coth(E_{00}/kT). \quad (10)$$

This means that the $\ln\{I_t/[1 - \exp(-qV/kT)]\}$ versus V plot should yield a straight line with slope giving E_0 and intercept at zero bias the saturation current I_{t0}. When E_0 values determined from experimental I–V data are fitted into equation (10), E_{00} turns out to be around 6.8 meV, an order of magnitude higher than the value estimated from equation (7). Hence the result appears to be inconsistent.

All the considerations advanced above suggest that tunnelling can become increasingly important only in highly doped semiconductors having $N_A > 10^{23}$ m^{-3}. At lower dopant concentrations, the contribution of tunnelling (FE and TFE) becomes insignificant and TED dominates.

Similarly, the recombination current can be described by [20]

$$I_r = I_{r0}\left[\exp\left(\frac{qV}{2KT}\right) - 1\right] \quad (11)$$

with

$$I_{r0} = qn_i A_d w/2\tau \quad (12)$$

and $n_i = (N_c N_v)^{1/2} \exp(-E_g/2kT)$. Here w is the thickness of the depletion region, τ is the carrier effective lifetime within the depletion region, n_i is the intrinsic carrier concentration, E_g is the energy bandgap and N_c and N_v are the effective conduction- and valence-band density of states respectively.

The recombination of the electrons and holes is normally most effective near the centre of the bandgap. Chen *et al* [15] have pointed out that if recombination current exists and is neglected, the barrier height evaluation on the basis of TED theory yields progressively lower values with decrease in temperature; for example if I_r constitutes 91% of the total current at (say) 100 K, the expected barrier decrease is 0.02 eV. This is the level of change actually observed in the present work (figure 2). However, such a possibility requires I_r to be of the same order as the current caused by the TED

mechanism. In other words, the saturation current I_{r0} should be $\sim 10^{-14}$ A as against the estimated value of 10^{-34} A using equation (12). Also, assuming the experimental current below 100 K to be just recombination current I_{r0}, the energy bandgap E_g can be determined from the slope of the $\ln(I_{r0}/T^{3/2})$ versus $1/T$ plot. This gives E_g as 0.5 eV, which is quite a low value. Moreover, the depletion region recombination current is expected to become important only for Schottky diodes with large barrier height, low temperatures and lightly doped semiconductors with low carrier lifetime [20]. Therefore, one may infer that recombination current is also insignificant in the present case.

The above considerations, together with the fact that the $\ln I$ versus V plot becomes increasingly straight covering a larger span with decrease in temperature, suggest that the thermionic emission–diffusion mechanism is indeed operative even below 84 K. Therefore, an apparent increase in η and decrease in barrier height at very low temperatures are possibly caused by some other effects (inhomogeneities of thickness and composition of the silicide layer, non-uniformity of the interfacial charges, etc) giving rise to extra current such that the overall characteristic still remains consistent with the thermionic emission process. The variation of series resistance (R_s) as a function of temperature is shown in figure 4. The sharp increase of R_s below 110 K is quite similar to the reported observations in a PtSi/silicon Schottky barrier diode and is believed to result from lack of free charge carriers at low temperatures [6].

The linear portion of the ϕ_{b0} versus T plot (figure 2) allows evaluation of the temperature dependence of the barrier height by writing

$$\phi_{b0}(T) = \phi_{b0}(0) + \alpha T \tag{13}$$

where α is the temperature coefficient of the barrier height. The fitting of the experimental data yields $\alpha = 1.49 \times 10^{-4}$ eV K^{-1} and $\phi_{b0}(0) = 0.33$ eV.

The barrier height can also be determined in yet another way. Equation (4) can be rewritten as

$$\ln(I_s/T^2) = \ln(A_d A^{**}) - \frac{q\phi_{b0}}{kT}. \tag{14}$$

Therefore, the $\ln(I_s/T^2)$ versus $1/T$ plot should, in principle, yield a straight line with slope determining the zero-bias barrier height (ϕ_{b0}) and the intercept at the ordinate giving the Richardson constant itself for a known diode area A_d. This method gives a single value of barrier height. Figure 5 shows the plot of $\ln(I_s/T^2)$ versus $1000/T$. The experimental data appear to fit, with two straight lines in different temperature regimes giving two activation energies (0.33 eV and 0.24 eV), instead of a single ϕ_{b0} predicted by the thermionic emission–diffusion theory. The value of A^{**} obtained from the intercept of the straight portion at the ordinate is equal to 5.8 A cm^{-2} K^{-2}, which is much lower than the known value of 32 A cm^{-2} K^{-2}. This is perhaps because equation (4) does not take into account the variation of the barrier height with temperature as exhibited in figure 2 and evaluated above using equation (13). By replacing ϕ_{b0} by $\phi_{b0}(T) = \phi_{b0}(0) + \alpha T$ in equation (4), the intercept of $\ln(I_s/T^2)$ versus $1000/T$ yields $\ln(A^{**}A_d) - \alpha q/k$. With the value of α obtained above as 1.49×10^{-4} eV K^{-1}, A^{**} comes out to be 33 A cm^{-2} K^{-2} which is indeed a significant improvement. Further, it turns out that the activation energy of 0.33 eV corresponds to the zero-bias barrier height ϕ_{b0} at zero temperature itself. Such an observation is always valid. The reason perhaps lies in both being derived from the same set of I_s data; while one is extracted from the slope of the straight line portion of the activation energy $\ln(I_s/T^2)$ versus $1/T$ plot, the

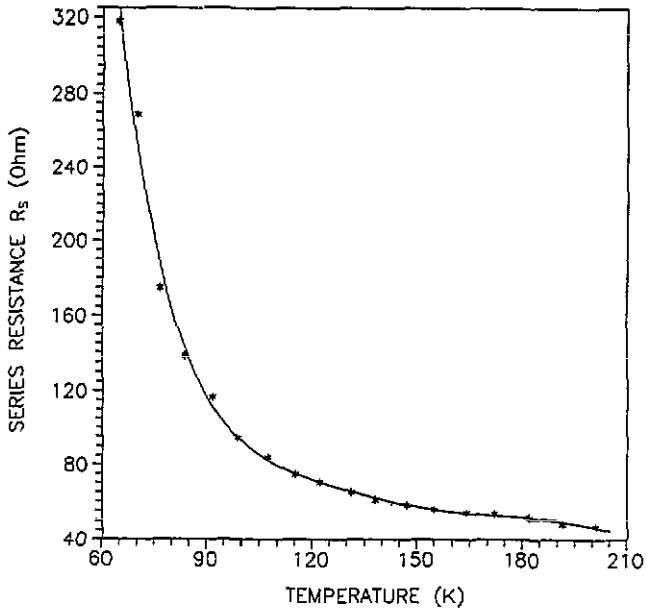

Figure 4. Temperature dependence of the series resistance R_s. It shows a sharp increase in R_s as the temperature falls below ~ 110 K.

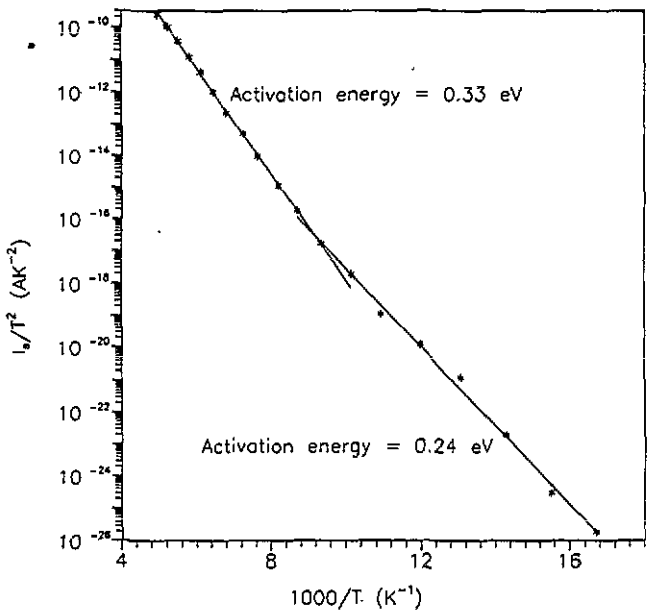

Figure 5. $\ln(I_s/T^2)$ versus $1000/T$ plot of a Pd_2Si/p-Si(111) Schottky barrier. It shows a best fit with two straight lines corresponding to activation energies of 0.33 eV and 0.24 eV.

other is found by extrapolation of the best fit straight line of the $\phi_{b0}(T)$ versus T plot at the ordinate, $\phi_{b0}(T)$ being determined using equation (4) in the corresponding range of temperatures only. Moreover, the results do confirm the dominance of the thermionic emission–diffusion current in Pd_2Si/p-Si Schottky barrier diodes in the temperature range 107–201 K.

4.1.2. The T_0 effect. The temperature dependence of the ideality factor η is usually taken as [21]

$$\eta = 1 + \frac{T_0}{T} \tag{15}$$

where T_0 is a constant. It is customary to plot ηT versus T. This, according to equation (15), should give a straight line of slope unity with an intercept at the ordinate the value of T_0. Figure 6 shows such a plot giving T_0 as 7 K but the slope 1.15 instead of unity. In fact, the slope nearly corresponds to the average value of η in the temperature range of interest. This suggests that for real Schottky diodes 'unity' in equation (15) be replaced by yet another constant η_0, the value of which can be obtained by the slope of the ηT versus T plot. The upward bending in the ηT versus T plot below 84 K is caused by apparent high values of η. The effect is such that the product ηT decreases rather slowly with decrease in T.

Also, a plot of $\ln(I_s/T^2)$ versus $1000/T$ shows non-linear behaviour in a certain temperature range, the reason being the decrease in barrier height and increase in ideality factor with fall in temperature. The effect is basically such that an extra current contribution results. Since in such situations the $\ln(I_s/T^2)$ versus $1000/\eta T$ plot sometimes gives a straight line, η is introduced in equation (4) to explain the observed behaviour such that I_s is

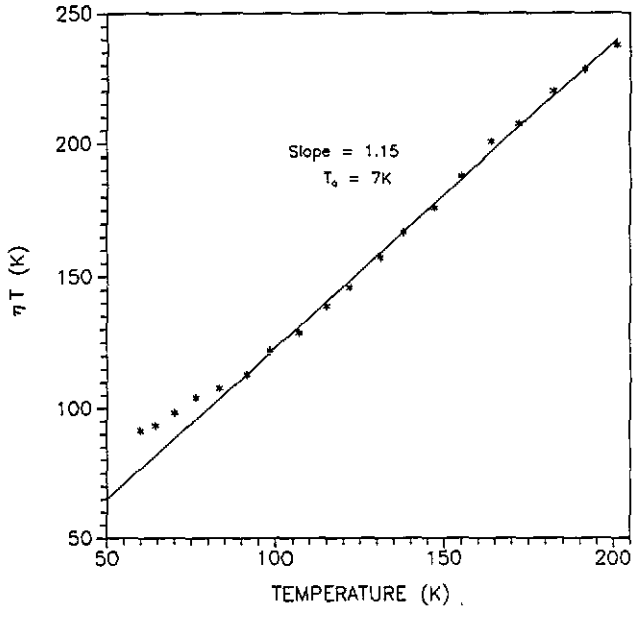

Figure 6. ηT versus T plot indicating the validity of the T_0 effect above ~84 K only. The deviation from the straight line at lower temperatures is due to a sharp increase in the value of η.

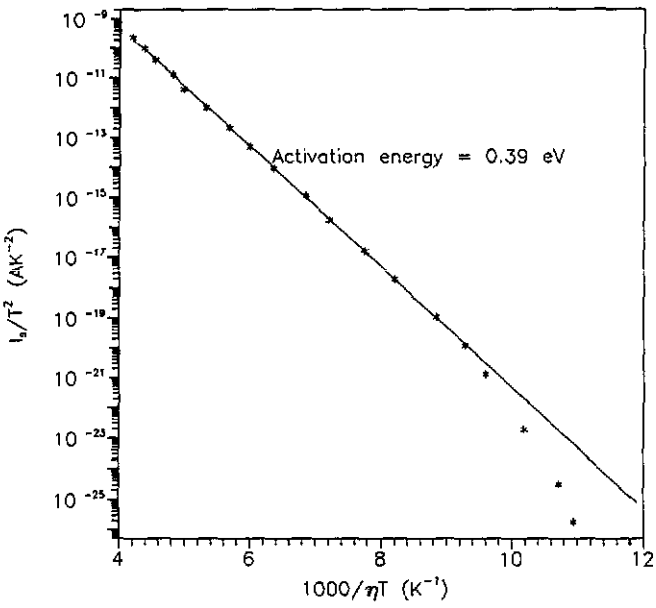

Figure 7. $\ln(I_s/T^2)$ versus $1000/\eta T$ plot of Pd_2Si/Si(111) Schottky barrier diodes. The extent of the linear portion no doubt increases (in comparison with figure 5) but data points now appear on the other side of the straight line in the low-temperature regime.

described by [21]

$$I_s = A_d A^{**} T^2 \exp\left(\frac{-q\phi_{b0}}{\eta kT}\right). \tag{16}$$

This means that as η is increasing with decrease in temperature, ϕ_{b0} is effectively reduced to ϕ_{b0}/η. Figure 7 shows a typical $\ln(I_s/T^2)$ versus $1000/\eta T$ plot. Such a consideration no doubt increases the range of linearity of the plot, but deviation still persists at very low temperatures (i.e. below 84 K). In fact, the correction applied seems to be much more than required for the observed current below 84 K, at least since the data points now lie on the other side of the line (figure 7). It may be noted that equation (16) is arrived at following the replacement of T by ηT or $T + T_0$ in equation (4) since $\eta T = T + T_0$. This is popularly referred to as the 'T_0 effect'. It is obvious from the results presented in figures 6 and 7 that the T_0 effect alone cannot account for the nonlinearity below 84 K, at least for Pd_2Si/p-Si Schottky barrier diodes. Needless to say there is no justification for the introduction of η in equation (4) to obtain equation (16). A slight improvement in the results by such a substitution possibly arisen in an unknown way rather artificially and requires further investigation for a proper explanation.

4.1.3. Flat-band barrier height. Another way to correlate the derived parameters η and ϕ_{b0} is to calculate the flat-band barrier height (ϕ_b^f). It is believed that ϕ_b^f is a real fundamental quantity and a better measure of barrier height. To find out the value of ϕ_b^f use is made of the expression [22]

$$\phi_b^f = \eta\phi_{b0} - (\eta - 1)(kT/q)\ln(N_V/N_A). \tag{17}$$

Figure 2 shows the variation of ϕ_b^f as a function of temperature. It is evident that ϕ_b^f is invariably larger than ϕ_{b0} and is almost constant over wide range of temperature (down to 76 K) unlike ϕ_{b0}. There is, however, a significant increase in ϕ_b^f values at temperatures below 76 K. This is possibly due to extremely high values of η. To be precise, ϕ_b^f can be assumed to vary with temperature above 76 K such that

$$\phi_b^f(T) = \phi_b^f(0) + \beta T \tag{18}$$

where $\phi_b^f(0)$ is the zero-temperature flat-band barrier height and β is the temperature coefficient of ϕ_b^f. The fitting of $\phi_b^f(T)$ data in equation (18) yields $\phi_b^f(0) = 0.401$ eV and $\beta = 2.21 \times 10^{-5}$ eV K^{-1}.

On writing ϕ_{b0} in terms of ϕ_b^f using expression (17), equation (4) becomes

$$I_s^f = A_d A^{**} T^2 \exp\left(\frac{-q\phi_b^f}{\eta kT}\right) \tag{19}$$

where

$$I_s^f = I_s \exp\left(\frac{\eta - 1}{\eta} \ln(N_V/N_A)\right) \tag{20}$$

is called the flat-band saturation current.

Unewisse and Storey [10] suggested a plot of $\eta \ln(I_s^f/T^2)$ versus $1/T$ for evaluation of the Richardson constant A^{**}. In that case the intercept at the ordinate gives $\eta \ln(A_d A^{**})$ and so some value of η is required for extracting A^{**}. Since η varies with temperature, a reliable measure of A^{**} with this method is not possible. Instead, a plot of $\ln(I_s^f/T^2)$ versus $1/\eta T$ according to equation (19) should also be a straight line with the slope directly yielding ϕ_b^f and the intercept $(=\ln(A_d A^{**}))$ at the ordinate determining A^{**} for a given diode area A_d. Figure 8 shows such a plot. A comparison with figure 5 reveals that the activation energy plot for flat-band saturation current becomes linear over a wide temperature range and deviates from a straight line only below 76 K. Moreover, it gives ϕ_b^f and A^{**} as 0.401 eV and 24.9 A cm^{-2} K^{-2} respectively. Taking into account the variation of ϕ_b^f with temperature as indicated in equation (18) one obtains a modified value of the Richardson constant $A^{**\prime} = A^{**} \exp(-\beta q/k)$ as 32.2 A cm^{-2} K^{-2}, in close agreement with the theoretical value of 32 A cm^{-2} K^{-2}.

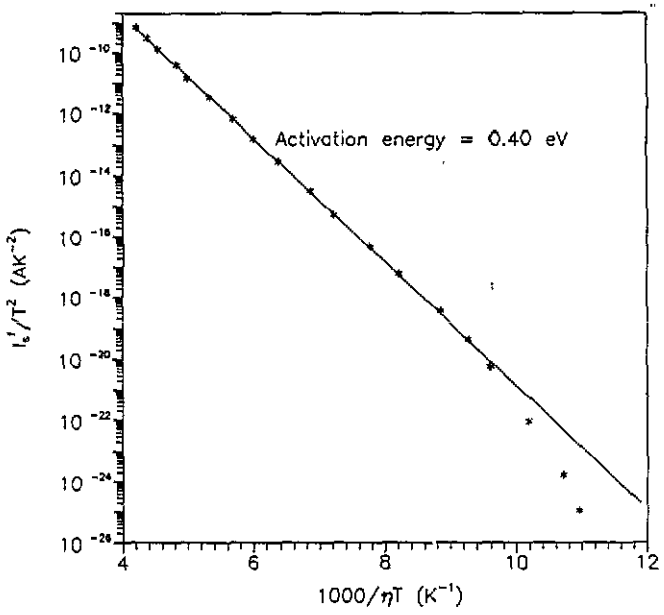

Figure 8. Activation energy plot of flat-band saturation current (I_s'). Notice its similarity to figure 7.

4.2. Reverse bias characteristics

According to the thermionic emission–diffusion theory, the reverse current (I_r) of a Schottky barrier diode should saturate at a value

$$I_r = A_d A^{**} T^2 \exp\left(\frac{-q\phi_{b0}}{kT}\right). \tag{21}$$

However, in practice, reverse characteristics do not show saturation due to the electric field dependence of barrier height, tunnelling, generation–recombination of electron–hole pairs in the depletion region, etc. All these factors cause additional current contributions precluding saturation. The effect of reverse bias V_r is to increase the electric field strength in the depletion region which, in turn, decreases the barrier height such that

$$\phi_{eff} = \phi_{b0} - \Delta\phi(V_r) \tag{22}$$

where ϕ_{b0} is the asymptotic value of Schottky barrier height at zero bias and $\Delta\phi(V_r)$ refers to the decrease in barrier height at a reverse bias V_r. The lowering of barrier height is attributed to image force, presence of an interfacial layer, etc. The contributions due to image force, $\Delta\phi_{if}$, and the interfacial layer present between the silicide and the semiconductor, $\Delta\phi_{il}$, are respectively given by [23]

$$\Delta\phi_{if} = \left(\frac{q^3}{8\pi^2\varepsilon_s^3}(N_A V_r)\right)^{1/4} \tag{23}$$

and

$$\Delta\phi_{il} = \alpha\left(\frac{2q}{\varepsilon_s}(N_A V_r)\right)^{1/2} \tag{24}$$

where α is a constant having dimensions of length and the other terms have their usual meanings. $\Delta\phi_{il}$ is larger than $\Delta\phi_{if}$ for large reverse bias V_r. The total lowering of the barrier height is thus

$$\Delta\phi = \Delta\phi_{if} + \Delta\phi_{il}. \tag{25}$$

By replacing ϕ_{b0} by ϕ_{eff} in equation (21) and entering the appropriate terms from expressions (23)–(25), the net reverse current is expressed as

$$I_r = A_d A^{**} T^2 \exp\left\{-\frac{q}{kT}\left[\phi_{b0} - \left(\frac{q^3}{8\pi^2\varepsilon_s^3}(N_A V_r)\right)^{1/4} - \alpha\left(\frac{2q}{\varepsilon_s}(N_A V_r)\right)^{1/2}\right]\right\} \tag{26}$$

or

$$\ln\left(\frac{I_r}{T^2}\right) = \ln(A_d A^{**}) - \frac{q}{kT}\left[\phi_{b0} - \left(\frac{q^3}{8\pi^2\varepsilon_s^3}(N_A V_r)\right)^{1/4} - \alpha\left(\frac{2q}{\varepsilon_s}(N_A V_r)\right)^{1/2}\right]. \quad (27)$$

If the plot of $\ln(I_r/T^2)$ versus $1/T$ gives a straight line for each bias V_r, the effective barrier height (ϕ_{eff}) can be found. As ϕ_{b0} is already known from the forward characteristics, reduction in barrier height can be easily determined since $\Delta\phi(V_r) = \phi_{b0} - \phi_{eff}$. The slope of the $\ln(\Delta\phi(V_r))$ versus $\ln V_r$ plot gives the exponent of V_r, indicating the dominance of the factor influencing the lowering of the barrier height.

Figure 9 shows the $\ln(I_r/T^2)$ versus $1000/T$ plots for Pd_2Si/p-Si Schottky barrier diodes. These clearly demonstrate that, at any given temperature, current is increasing with the level of reverse bias. Also, linearity over a certain temperature range indicates that the thermionic emission–diffusion mechanism is operative in the reverse bias mode as well. Tunnelling is the main cause of soft reverse I–V characteristics [20]. Also, the surface/edge effects give rise to additional current by a tunnelling mechanism in Schottky diodes. Figure 9 shows an activation energy plot depicting the deviation from the straight line for bias values 0.5–5 V. There is shift of the turning point towards higher temperature with an increase in the level of reverse bias. Obviously, the effect is greater at higher reverse bias. However, consideration here is limited to the portion up to the turning point at each bias, i.e. the regime where thermionic emission is dominant. The tunnelling contribution and surface/edge

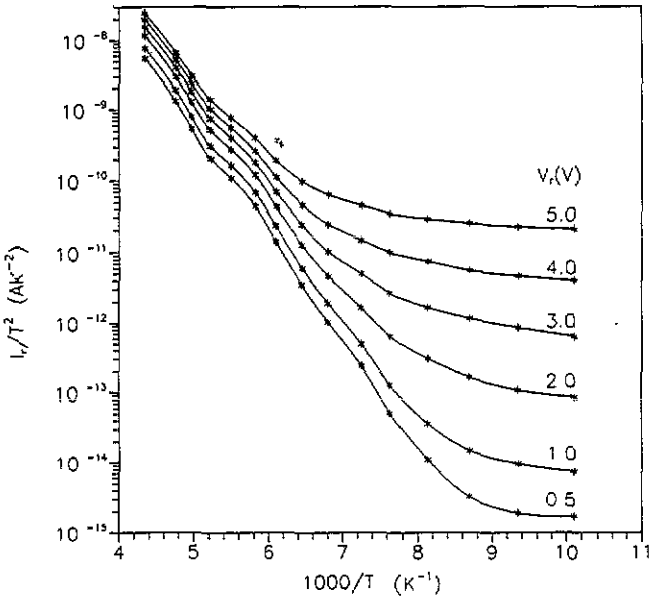

Figure 9. $\ln(I_r/T^2)$ versus $1000/T$ plot of Pd_2Si/p-Si Schottky barrier diodes under various reverse bias conditions. It shows saturation with a span extending progressively towards higher temperatures with the level of reverse bias.

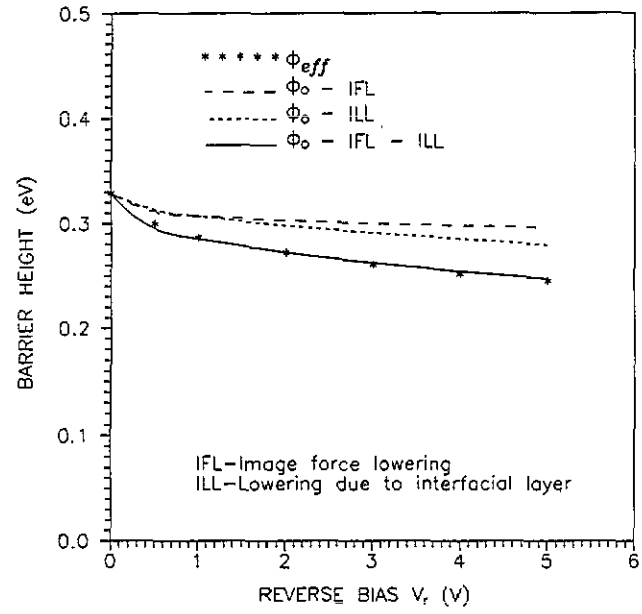

Figure 10. Effective barrier height as a function of reverse bias in Pd_2Si/p-Si Schottky barrier diodes along with lowering effects due to image force and the interfacial layer (with $\alpha = 56$ Å), taken individually and together.

effects have therefore been ignored in the region of interest. In all, four samples were investigated. They were similar with a variation in values lying within the experimental error.

The effective barrier height ϕ_{eff} as estimated from the gradient of the straight line portion of the $\ln(I_r/T^2)$ versus $1000/T$ plot at each reverse bias V_r is shown in figure 10 along with the corresponding values determined by consideration of lowering of barrier height due to image force $\Delta\phi_{if}$ and the presence of an interfacial layer $\Delta\phi_{il}$ using expressions (23) and (24) respectively and taking ϕ_{b0} as the zero-bias barrier height evaluated from the forward bias I–V characteristics. Clearly, the image force lowering alone is inadequate to account for the decrease in barrier height. However, incorporating effect of both the interfacial layer and image force lowering the observed barrier height reduction can be explained using equations (23)–(25) with $\alpha = 56$ Å.

Figure 11 shows the $\ln(\Delta\phi(V_r))$ versus $\ln V_r$ plot along with the theoretical curves of barrier reduction due to image force and the presence of an interfacial layer with the slope giving the exponent of V_r as $n = 1/2.2$. This value is somewhat nearer to 1/2, indicative of the dominance of interfacial layer effects in causing the lowering of barrier height in the reverse bias mode. Needless to say, Andrews and Lepselter [24] explained the reverse bias characteristics of Rh, Zr, and Pt silicide-based Schottky barrier diodes by assuming a linear field dependence such that $\Delta\phi \propto V_r$. Also, Fugita *et al* [23] have reported exponent values of nearly 1/2 whereas the results of Hodson *et al* [25] correspond to a somewhat higher value of the exponent for Schottky contacts on AlInAs layers.

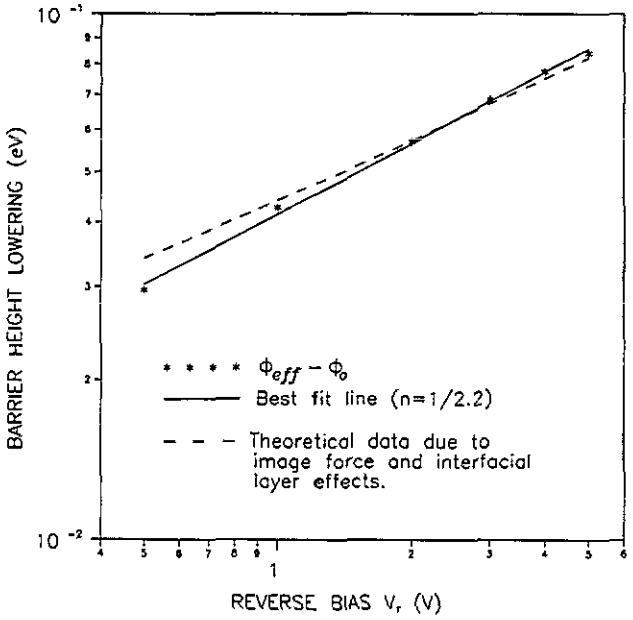

Figure 11. Barrier height reduction ($\Delta\phi$) as a function of reverse bias (V_r). The theoretical data are obtained by considering image force lowering and interfacial layer effects simultaneously with $\alpha = 56$ Å.

5. Conclusions

(i) I–V characteristics of the Pd_2Si/p-Si(111) Schottky barriers follow a thermionic emission–diffusion mechanism under both forward and the reverse bias conditions.

(ii) Forward I–V characteristics reveal that while the zero-bias barrier height ϕ_{b0} decreases, the ideality factor η and series resistance R_s increase with decrease in temperature. Moreover, the changes in ϕ_{b0}, η and R_s become quite significant at very low temperatures.

(iii) The zero-bias barrier height at absolute zero is found to be $\sim$0.33 eV with a temperature coefficient of 1.49×10^{-4} eV K^{-1}. The $\ln(I_s/T^2)$ versus $1000/T$ plot fits well, with two straight lines in different temperature regimes giving activation energies of 0.33 eV (201–107 K) and 0.24 eV (below 107 K) respectively and the value of the effective Richardson constant as 33 A cm^{-2} K^{-2}.

(iv) The T_0 effect cannot account for the apparent increase of ideality factor and decrease of barrier height with a fall in temperature below $\sim$100 K. Such changes are possibly caused by some other effects (inhomogeneities of thickness and composition of silicide layer, non-uniformity of the interfacial charges, etc) that give rise to extra current resulting in the overall characteristics still consistent with the thermionic emission–diffusion process.

(v) The flat-band barrier height at absolute zero as derived from the data is 0.401 eV with a temperature coefficient of 2.21×10^{-5} eV K^{-1}. Further, an $\ln(I_s^1/T^2)$ versus $1000/\eta T$ plot is suggested to obtain the value of the flat-band barrier height and effective Richardson constant; the corresponding values obtained are 0.401 eV and 32.2 A cm^{-2} K^{-2} respectively.

(vi) The decrease of barrier height with voltage under reverse bias is attributed mainly to the interfacial layer effects with a small contribution due to image force lowering.

References

[1] Elabd H, Villani T S and Kosonocky W F 1982 *IEEE Trans. Electron Devices Lett.* **3** 89–90
[2] Kosonocky W F and Elabd H 1983 *Proc. SPIE* **443** 167
[3] Kosonocky W F, Shallcross F V, Villani T S and Groppe J V 1985 *IEEE Trans. Electron Devices* **32** 1564–73
[4] Wittmer M 1990 *Phys. Rev.* B **42** 5249–59
[5] Wittmer M 1991 *Phys. Rev.* B **43** 4385–95
[6] Donoval D, Barus M and Zdimal M 1991 *Solid-State Electron.* **34** 1365–73
[7] Chin V W L, Green M A and Storey J W V 1993 *Solid-State Electron.* **36** 1107–16
[8] Chin V W L, Green M A and Storey J W V 1990 *Solid-State Electron.* **33** 299–308
[9] Barus M and Donoval D 1993 *Solid-State Electron.* **36** 969–74
[10] Unewisse M H and Storey J W V 1993 *J. Appl. Phys.* **73** 3873–9
[11] Duboz J Y, Badoz P A, Avitaya F and Rosencher E 1990 *J. Electron. Mater.* **19** 101–4
[12] Aboelfotoh M O 1991 *Solid-State Electron.* **34** 51–5
[13] Aboelfotoh M O, Cros A, Svensson B G and Tu K N 1990 *Phys. Rev.* B **41** 9819–27
[14] Aboelfotoh M O 1988 *J. Appl. Phys.* **64** 4046–55
[15] Chen T P, Lee T C, Ling C C, Beling C D and Fung S 1993 *Solid-state Electron.* **36** 949–54
[16] Chin V W L, Storey J W V and Green M A 1991 *Solid-State Electron.* **34** 215–16
[17] Werner J H and Guttler H H 1993 *J. Appl. Phys.* **73** 1315–19
[18] Chand S and Kumar J 1995 *Solid-State Electron.* **38** 1103–4
[19] Sze S M 1981 *Physics of Semiconductor Devices* 2nd edn (New York: Wiley) pp 255–8
[20] Rhoderick E H and Williams R H 1988 *Metal–Semiconductor Contacts* 2nd edn (Oxford: Clarendon)
[21] Saxena A N 1969 *Surf. Sci.* **13** 151–71
[22] Wagner L F, Young R W and Sugerman A 1983 *IEEE Trans. Electron Devices Lett.* **4** 320–2
[23] Fujita S, Naritsuka S, Noda T, Wagai A and Ashizawa Y 1993 *J. Appl. Phys.* **73** 1284–7
[24] Andrews J M and Lepselter M P 1970 *Solid-State Electron.* **13** 1011–23
[25] Hodson P D, Wallis R H, Davies J I, Riffat J R and Marshall A C 1988 *Semicond. Sci. Technol.* **3** 1136–8